



Temporal and spatial variations of dust deposition along a Red Sea coastal section

Item Type	Preprint
Authors	Shevchenko, Illia;Engelbrecht, Johann;Mostamandi, Suleiman;Stenchikov, Georgiy L.
Eprint version	Pre-print
Publisher	Submitted to European Geosciences Union
Journal	Submitted to Atmospheric Chemistry and Physics
Rights	Archived with thanks to European Geosciences Union
Download date	2024-04-17 06:04:53
Link to Item	http://hdl.handle.net/10754/664978

Figures

Temporal and spatial variations of dust deposition along a Red Sea coastal section

Illia Shevchenko¹, Johann P. Engelbrecht^{1,2}, Suleiman Mostamandi¹, and Georgiy Stenchikov¹

¹King Abdullah University of Science and Technology (KAUST), Physical Science and Engineering Division (PSE), Thuwal, 23955-6900, Saudi Arabia.

²Desert Research Institute (DRI), Reno, Nevada 89512-1095, U.S.A.



Fig. 1. Inverted Frisby aerosol deposition gauge, with polyester foam insert to prevent dust deposits being blown out once deposited in the dish. Also shown are spikes and fishing lines to discourage birds wanting to land on the sampler.

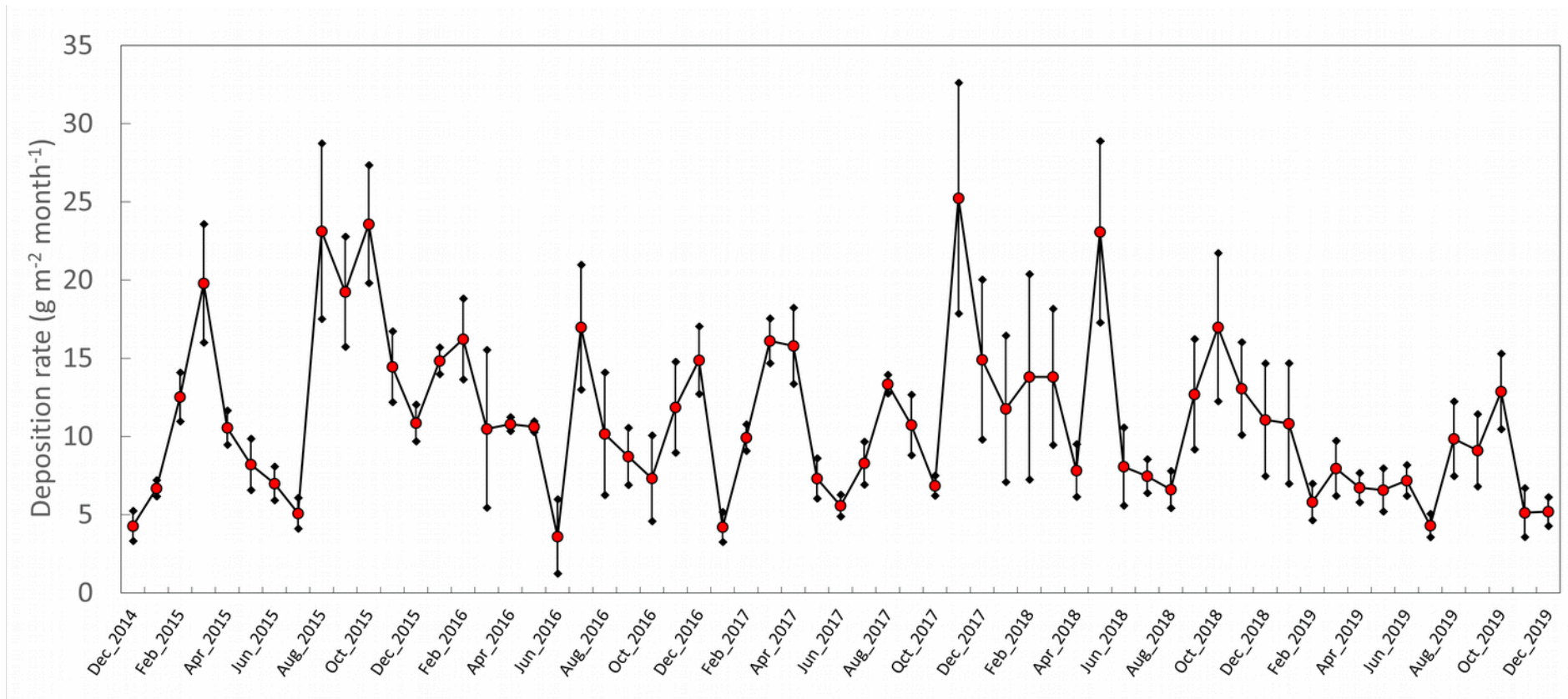


Fig. 2. Monthly averaged deposition rates from Frisbee deposition samplers. Error bars are one standard deviation about the monthly means.

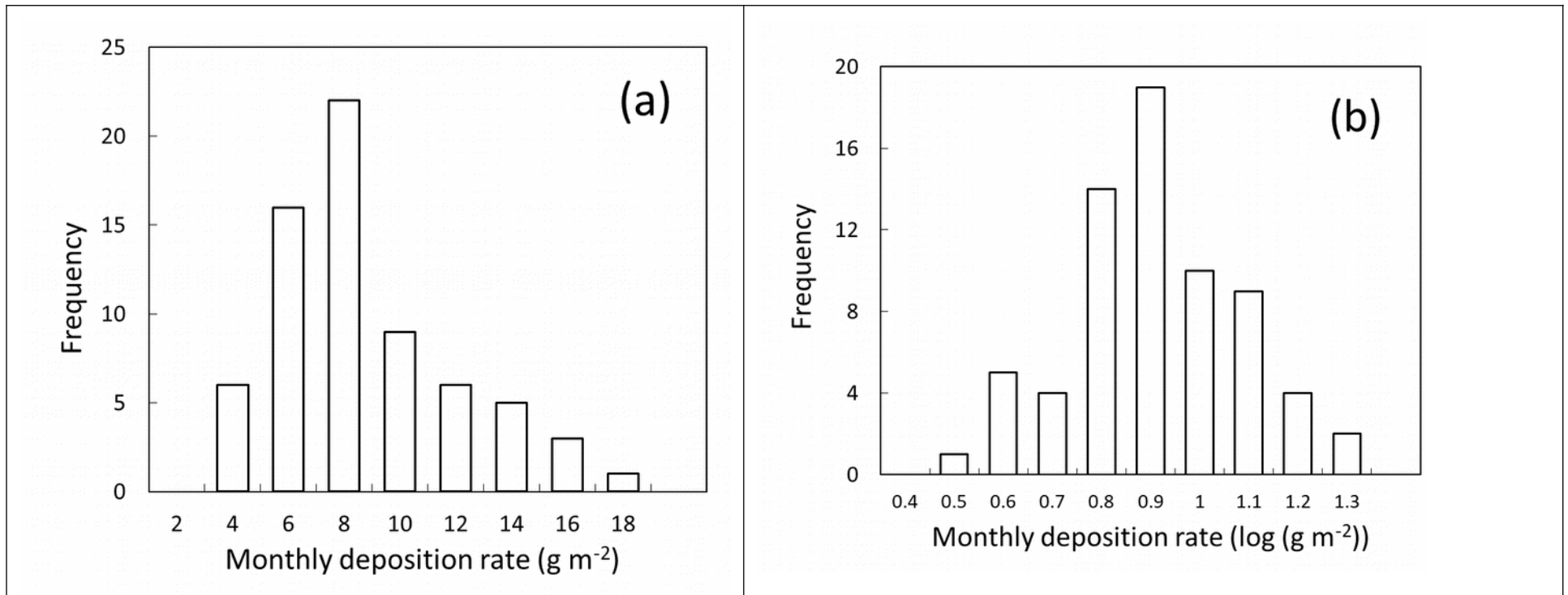


Fig 3. Histograms of (a) untransformed positively skewed monthly deposition rates, and (b) logarithmically transformed deposition rates showing a closer to normal distribution.

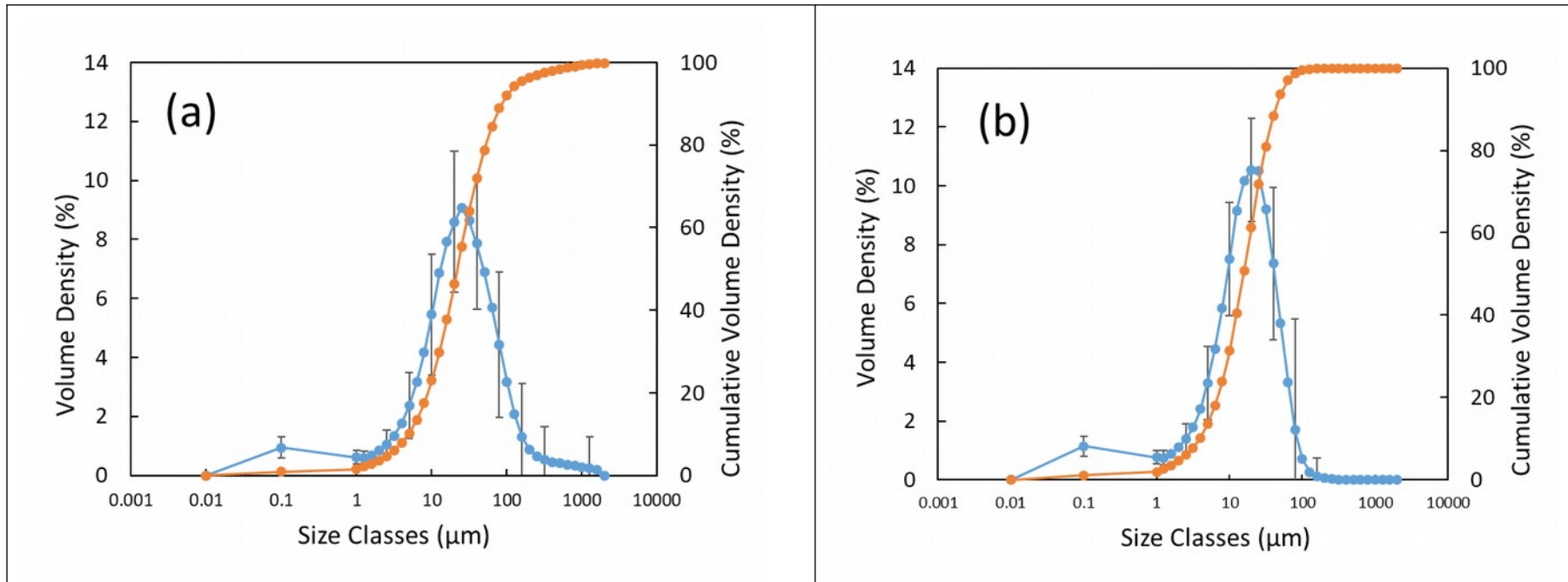


Fig. 4. Average volume distribution plots and standard deviations of 38 pairs of deposition samples collected over the period May 2016 to September 2018: (a) unsieved and (b) retroactively sieved.

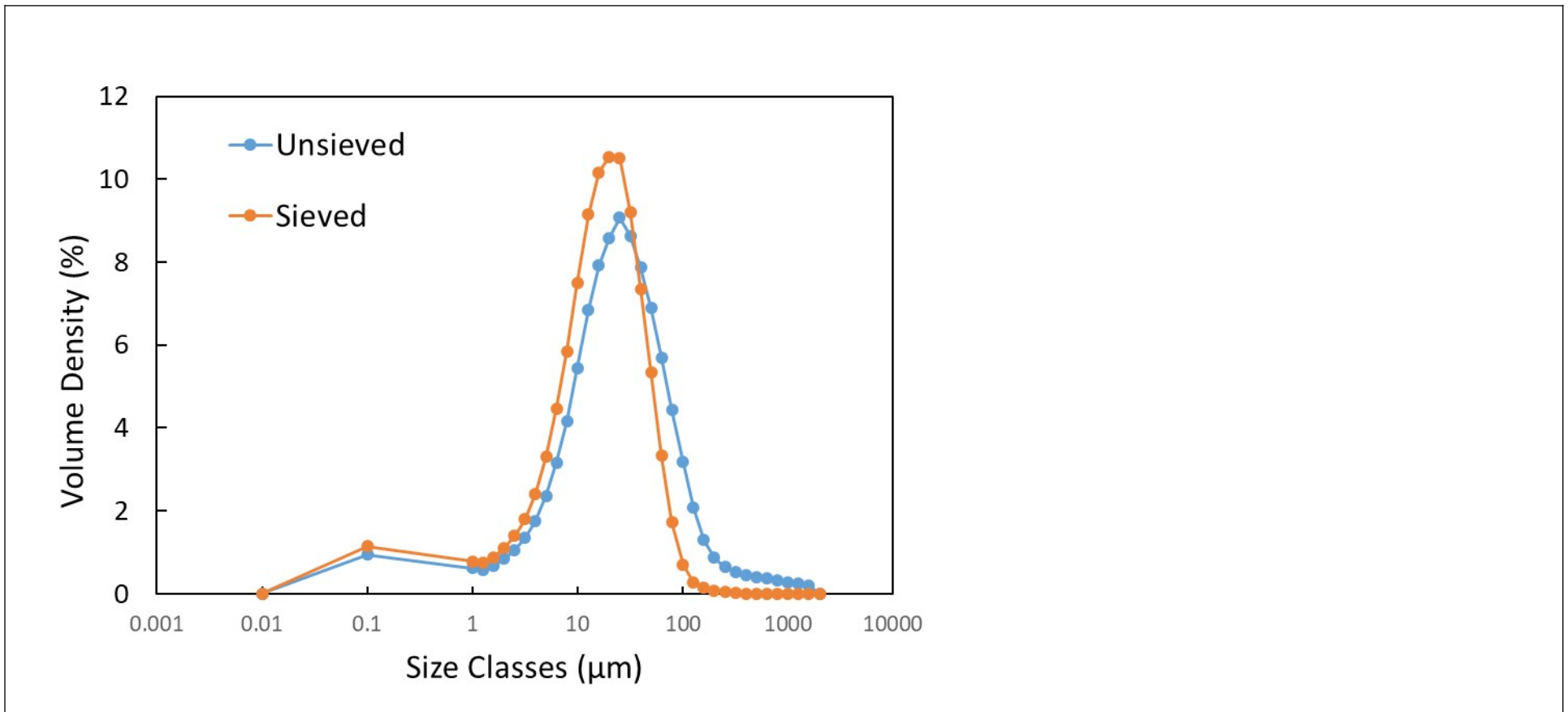


Fig. 5. Displacement of particle size distribution towards the smaller size bin, following the additional step of re-suspension, sieving to <math><56 \mu\text{m}</math>, and second particle size distribution measured on 38 samples.

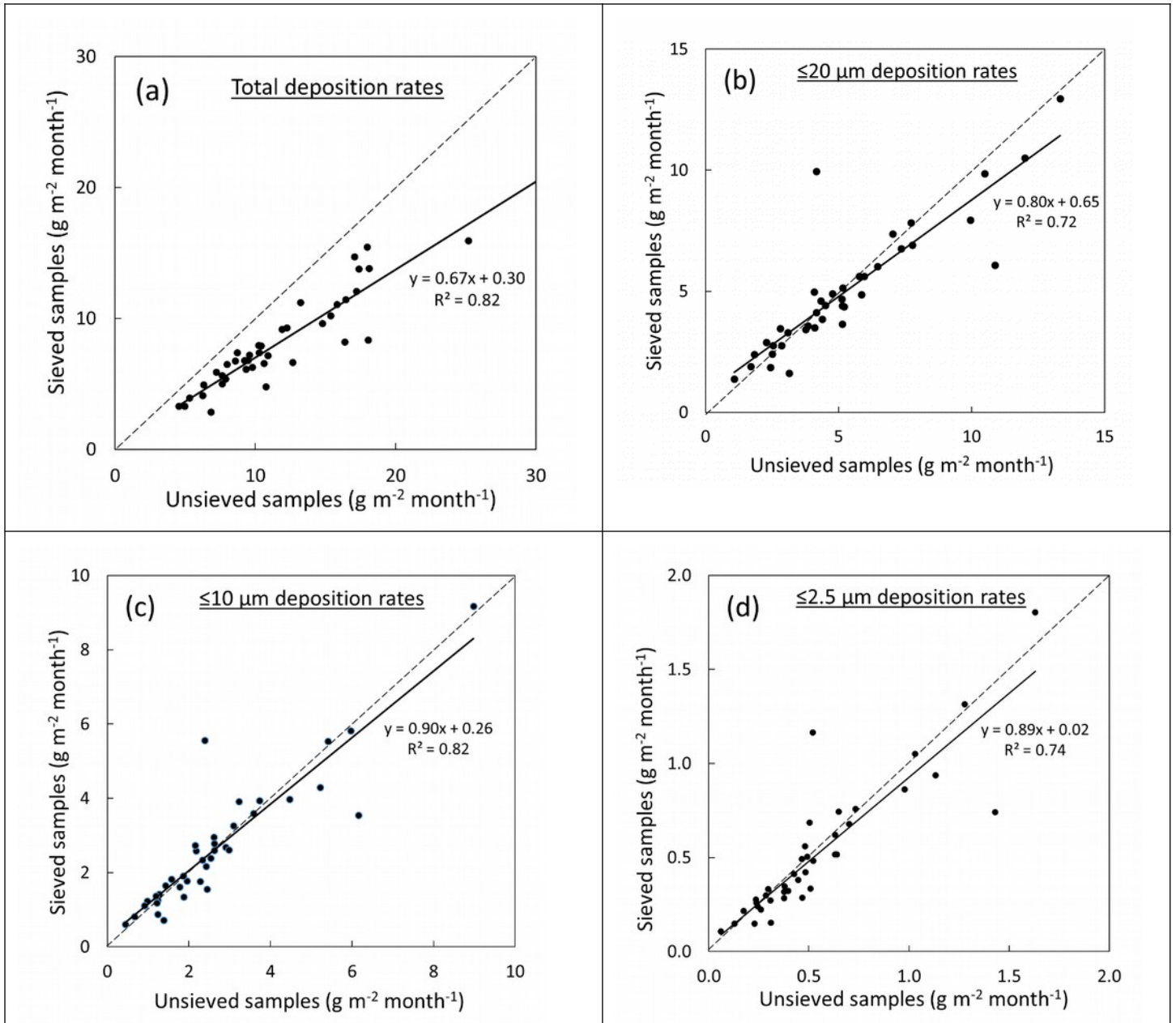


Fig 6. Comparative deposition rates ($\text{g m}^{-2} \text{ month}^{-1}$) prior and after resuspension in water and sieving to $<56 \mu\text{m}$ (a) total sample, (b) $\leq 20 \mu\text{m}$, (c) $\leq 10 \mu\text{m}$ and (d) $\leq 2.5 \mu\text{m}$ size fractions, as derived from individual sample distribution plots. Also shown are the 1:1 stippled lines.

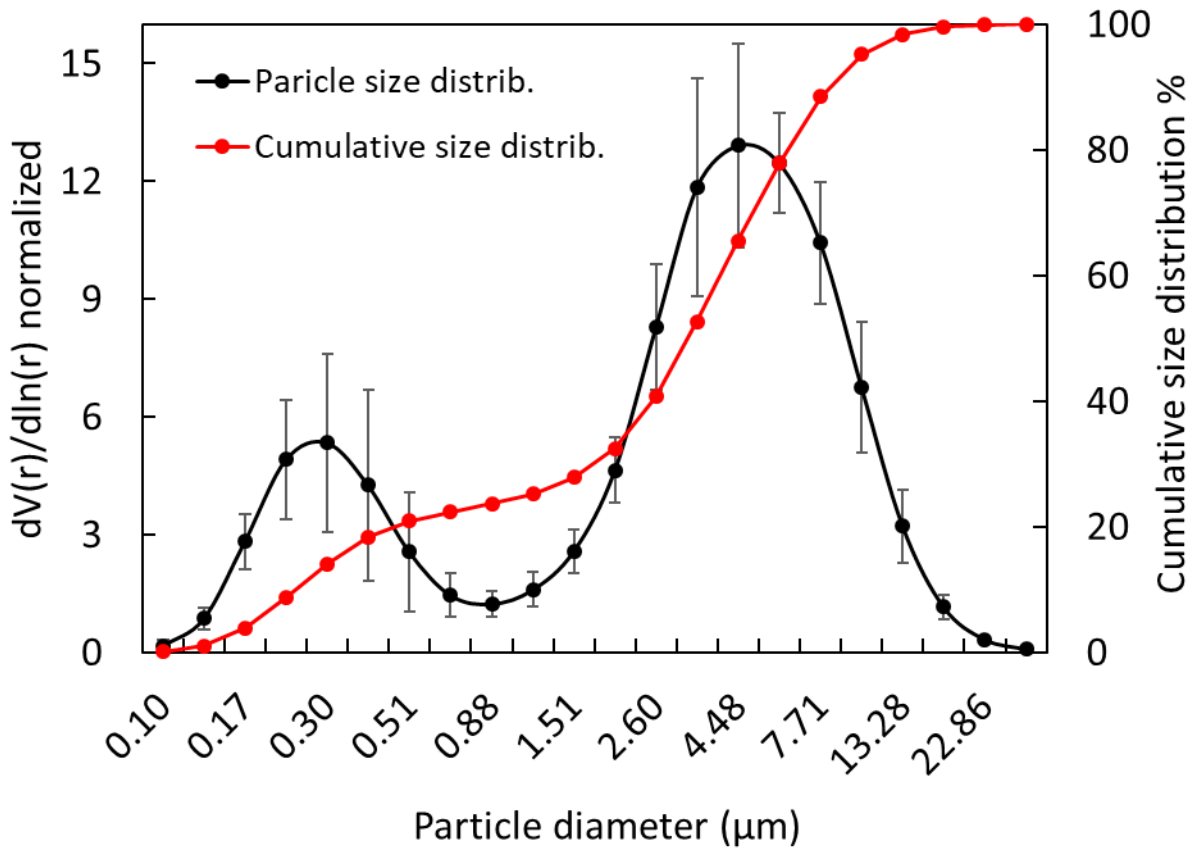


Fig. 7. Monthly average AERONET derived particle size distributions, with standard deviation per bin size, and cumulative volumes, for 19 sets of month-long measurements collected over the period July 2016 to September 2019. The bimodal lognormal distribution represents the peaks for fine and coarse modes of the aerosols, separated by a local minimum diameter at 0.88 μm .

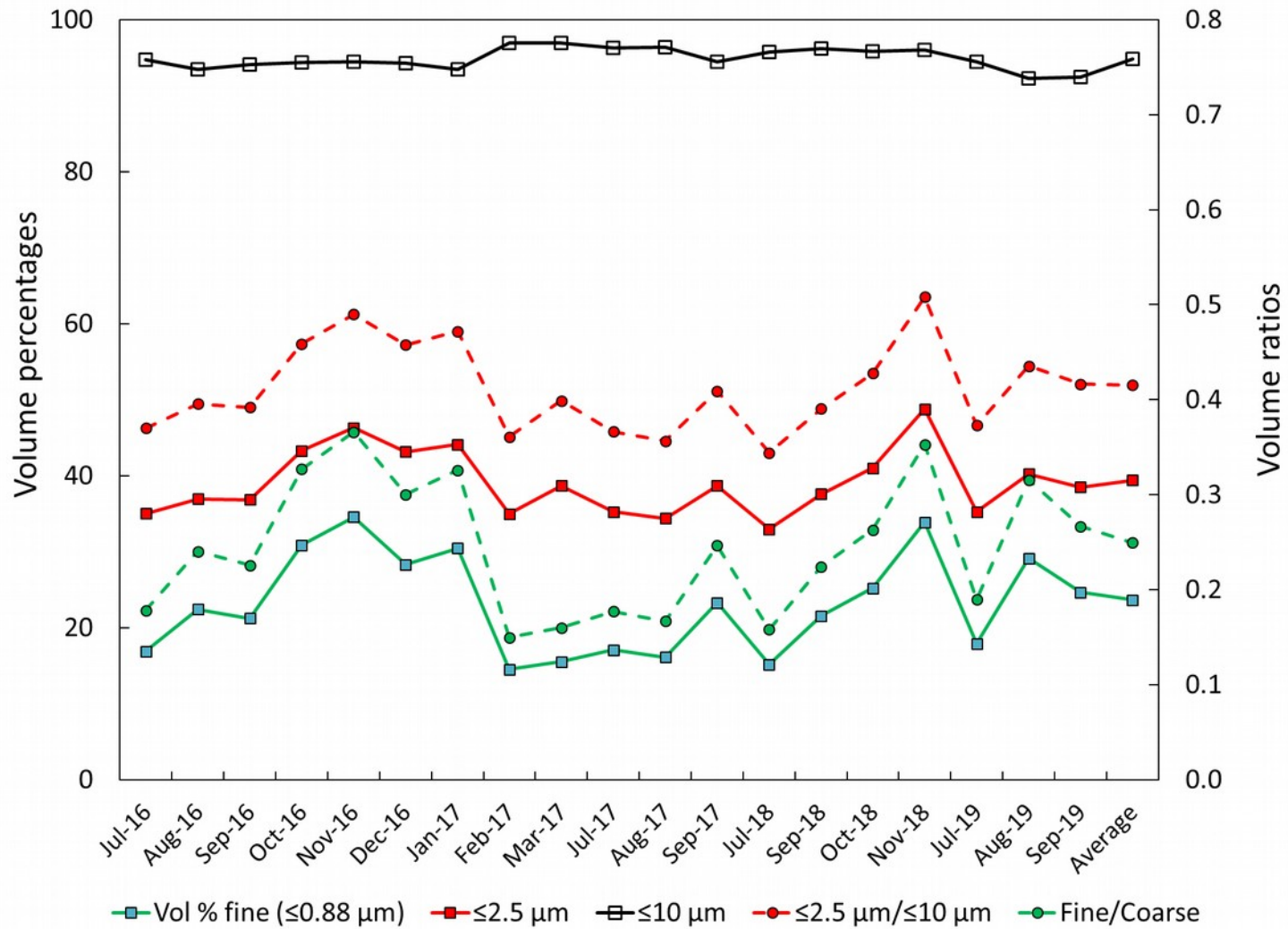


Fig. 8. Volumetric percentages derived from AERONET month long particle size distributions. Shown here are the $\leq 0.88 \mu\text{m}$, $\leq 2.5 \mu\text{m}$ and $\leq 10 \mu\text{m}$ volumetric percentages as well as their volumetric ratios. $\leq 2.5 \mu\text{m} / \leq 10 \mu\text{m}$ ratios can be interpreted as proxies for $\text{PM}_{2.5} / \text{PM}_{10}$ particulate ratios. Similarly the $\leq 0.88 \mu\text{m} / \leq 10 \mu\text{m}$ can be interpreted as Fine/Coarse volumetric (mass) ratios.

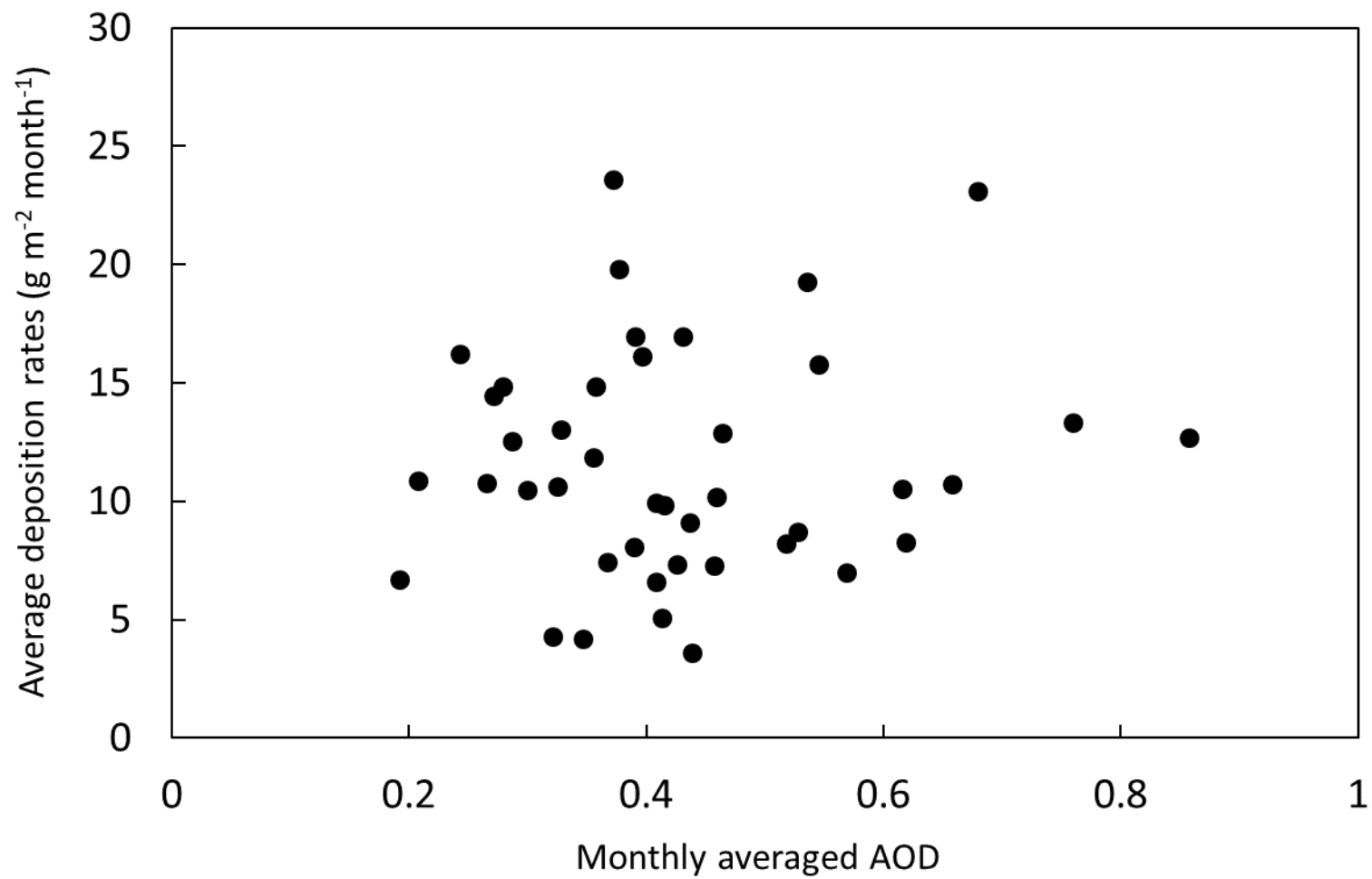


Figure 9. Comparison between monthly averaged deposition rates and monthly averaged aerosol optical depth (AOD) for 42 sample pairs collected in the period December 2014 to December 2019.